Contrib Mineral Petrol (1996) 123: 22–39

Peter S. Dahl

The crystal-chemical basis for Ar retention in micas: inferences from interlayer partitioning and implications for geochronology

Received: 9 February 1995 / Accepted: 8 September 1995

Abstract Cation partitioning data for coexisting muscovite and biotite are shown to be useful indicators of relative interlayer bond length/strength in these minerals. These data therefore provide a useful crystal-chemical perspective on relative mass-transfer kinetics of radiogenic isotopes, and account for the observation that biotite is generally less retentive of ^{40}Ar and ^{87}Sr than coexisting muscovite. Partitioning behavior of trace elements underscores three reasons why overall interlayer bonding in biotite is weaker than in muscovite. *First*, the preferences of large $(Rb, Cs)^{+}$ in biotite and of small La^{3+} and Na^{+} in muscovite indicate a relatively spacious interlayer volume in biotite (suggesting a longer mean K−O bond). *Second*, the preference of interlayer vacancies in biotite (with some/all possibly H_2O/H_3O^{+}-filled) suggests that its adjacent 2:1 sheets are connected by fewer interlayer bonds per unit cell than those of muscovite. *Third*, the relative exclusion of large Ba^{2+} from biotite despite its large interlayer sites is attributed to O−H bonds pointing into the interlayer cavity sub-normal to (001); (K^{+}, Ba^{2+})-H^{+} repulsion thereby induced by the bare proton both destabilizes Ba^{2+} and weakens K−O bonds. In contrast, muscovite offers a more favorable electrostatic environment for Ba^{2+} substitution since its O−H bonds are directed into the vacant M_1 octahedral site sub-parallel to (001). This hypothesis is supported by the observation that progressive $F(OH)_{-1}$ exchange enhances Ba^{2+} partitioning into biotite/phlogopite relative to coexisting muscovite. These crystal-chemical differences between biotite and muscovite are mirrored in calculated values of "ionic porosity", Z_i, defined here as the percentage of their interlayer unit-cell volume not occupied by ions. A monitor of ionic packing density and geometry, Z_i is inversely correlated with K−O bond strength, which appears to be the rate-determining "kinetic common denominator" for a variety of processes affecting micas – including those responsible for loss of radiogenic isotopes in biotite and muscovite. Accordingly, the relatively longer/weaker K−O bonds of biotite are envisioned as being more easily stretched (during volume diffusion) or broken (during recrystallization or retrograde alteration). This in turn accounts for common observations of enhanced radiogenic Ar/Sr loss and younger $^{40}Ar/^{39}Ar$ and Rb/Sr ages in natural biotite (high Z_i) relative to coexisting muscovite (lower Z_i). Significantly, this pattern may arise irrespective of isotopic loss mechanism (diffusion or recrystallization, etc.), and it follows that any age discordance observed between muscovite and biotite cannot be ascribed uniquely to one mechanism or the other without appropriate field, petrographic, and petrologic constraints. Extension of this partitioning/porosity-based synthesis leads to prediction of corollary age-retentivity-composition effects among chemically diverse trioctahedral and dioctahedral micas, which are best field tested in terranes that cooled slowly under dry, static conditions. Pressure effects on argon retention are also inferred from the porosity model.

P.S. Dahl (✉)
Department of Geology, Kent State University, Kent, OH 44242, USA

Editorial responsibility: V. Trommsdorff

Introduction

Biotite and muscovite are common and widespread in diverse lithologies, and their usefulness in studies of orogenic pressure-temperature-time evolution is well known (e.g., Guidotti 1984; Faure 1986; McDougall and Harrison 1988; Hoisch 1989; and many others). Many geochronologic studies have shown that biotite loses radiogenic Ar/Sr (or gains excess Ar) more readily than coexisting muscovite, despite exposure of both minerals to uniform metamorphic conditions. Relative to muscovite, therefore, metamorphic biotite typically yields either: (1) somewhat younger cooling ages ($^{40}Ar/^{39}Ar$, McDougall and Harrison 1988; Rb/Sr, Cliff et al. 1985), or (2) anomalously old *apparent* ages (both K−Ar and

Table 1 Diffusivities (D) of O and Ar inferred from hydrothermal bomb experiments on K-bearing micas

End member	D (cm^2/sec)[a] ($\times 10^{-17}$)	Z_i (%)[b]	Reference
Biotite	220 (oxygen)	48–49	Fortier and Giletti 1991
Muscovite	70 (oxygen)	45–46	Fortier and Giletti 1991
Phlogopite (F-rich)	20 (oxygen)	46–48	Fortier and Giletti 1991
Biotite	385 (argon)	48–49	Harrison et al. 1985
Muscovite	8 (argon)	45–46	Hames and Bowring 1994
Phlogopite (F-rich)	3 (argon)	46–48	Giletti 1974a

[a] T=500° C; P=1000 bars; infinite cylinder; (001) plane. The D value quoted for Ar in muscovite used diffusion parameters (E, D_o) recalculated by Hames and Bowring (1994), based upon original diffusion data of Robbins (1972)
[b] Z_i=interlayer ionic porosity at room conditions, estimated (this study) for compositions used in diffusion experiments; see text

$^{40}Ar/^{39}Ar$; e.g., Brewer 1969; Foland 1983; Dallmeyer and Gee 1986).

Specific reasons for the differing isotopic retention properties of biotite and muscovite have not been explored, despite general awareness among geochronologists that the kinetics of isotopic mass transfer is somehow rooted in crystal chemistry. In fact, most dating projects have other objectives and so are not directly concerned with this subject. However, establishing a crystal-chemical framework for isotopic retention (and thus for the diffusional closure process itself), in minerals has practical implications for geochronology, pursuant to potential refinements in post-orogenic cooling histories. This goal appears within reach for amphiboles, based upon preliminary ^{40}Ar retention modeling and its field testing (Dahl et al. 1995; Dahl in press; Kamber et al. 1995). Likewise, diverse mica compositions are accommodated by a flexible silicate structure (Bailey 1984; Guidotti 1984; Guggenheim 1984; Giese 1984), which on crystal-chemical grounds arouses suspicions of an age-retention-composition relationship parallel to that emerging in amphiboles. For micas we wish to understand age differences (both real and apparent): (1) between coexisting muscovite and biotite in a *given* rock, and (2) among compositionally diverse trioctahedral (or dioctahedral) varieties in *adjacent* rocks.

This paper begins the systematization of age-retentivity-composition links in micas by focusing on the basic crystal-chemical differences between biotite and muscovite – as specifically revealed by interlayer partitioning data. The logic of this approach follows from the fact that both non-random partitioning of cations and varying diffusivity of Ar/Sr share a common origin in the contrasting crystal fields of these coexisting micas (Dahl et al. 1993). Special focus on *interlayer*-site energetics is justified for two reasons. *First*, micas display pronounced diffusional anisotropy of O and Ar, with fastest diffusion in the relatively open interlayer region (see Giletti 1974a; Phillips and Onstott 1988; Onstott et al. 1991; Fortier and Giletti 1991; Hames and Bowring 1994) highlighted in Fig. 1 for phlogopite, $KMg_3AlSi_3O_{10}(OH)_2$. This anisotropy reflects the relative weakness of K−O bonds in the overall structure (see also Vaughan and Guggenheim 1986), which is further evidenced by the occurrence of interlayer cleavage and slip (Baños et al. 1983; Meike 1989). Isotopic mass transfer processes – i.e., volume diffusion, recrystallization, and reaction (Giletti 1974b; Graham and Elphick 1991) – all involve thermally activated stretching and/or reconstruction of chemical bonds (see Lasaga 1981; Putnis 1992). Mean K−O bond strengths, therefore, are potentially rate determining to these processes in that the basal planes collectively offer a parallel "path of least resistance" (Lasaga 1981) to transformation. *Second*, order-of-magnitude variations in interlayer O and Ar diffusivity among micas at 500° C (inferred here from published data; see Table 1) suggest further differences in K−O bond length/strength according to composition. This implies a corresponding link between composition and the kinetics of isotopic loss processes rate-limited by K−O bond strength. In particular, relatively weak interlayer bonds should present small kinetic barriers to transformation according to Arrhenius-type expressions (e.g., see Hanson and Gast 1967; Manning 1974; Giletti 1974a, b; Rubie and Thompson 1985; Kronenberg et al. 1990). A corollary expectation is that radiometric ages of coexisting micas will vary according to composition (and K−O bond strength) – all other factors equal.

In the first section of this paper, interlayer-species partitioning behavior supported by crystallographic data are used to establish the key crystal-chemical reasons for K−O bond length/strength differences between biotite and muscovite. Augmenting this outline is a new crystal-chemical explanation for the partitioning behavior of Ba^{2+} in terms of relative hydroxyl orientations in these micas. Postulated differences in their interlayer crystal fields (i.e., bond lengths, strengths, and angles) are approximated by the geometric parameter, ionic porosity (Z_i), defined here as the percentage of interlayer unit-cell volume not occupied by ions (cf., the more general definitions of Dowty 1980 and Fortier and Giletti 1989). The second section of the paper explores differential kinetic responses of biotite and muscovite to a host of processes – including those potentially responsible for isotopic loss and radiometric age discordance (see above) – and systematizes this behavior and its effect on age in terms of

the *Z*-based crystal-chemical framework developed earlier. In the final section, corollary differences among members of both the trioctahedral and dioctahedral mica families are also explored within this framework.

Interlayer partitioning data as a guide to relative K−O bond strengths in coexisting micas

Structural considerations

The true-mica structure consists of parallel T−O−T sheets (2:1 layers) alternating with layers of large alkali cations, as represented by phlogopite in Fig. 1 (see reviews by Bailey 1984; Guidotti 1984; and Giese 1984). Ionic bonds between these cations and basal oxygens in the tetrahedral layer connect adjacent T−O−T sheets. Interlayer K^+ (and/or Na^+) ideally occupies a di-hexagonal cavity defined by these oxygens, but structural misfit between the tetrahedral and smaller octahedral layers in natural micas necessitates counter-rotation of adjacent tetrahedra (Fig. 1, inset). Increased tetrahedral rotation progressively shrinks the K−O polyhedron into more of a ditrigonal antiprism. The resultant α-rotation angle (Fig. 1) exhibited by a given mica is controlled by its composition; that is, it depends mostly upon the *a*–*b* dimensions and relative bond lengths in the T−O−T layers (but also upon the identity of the interlayer cation; Bailey 1984). The α-rotation angle is important to this study because it correlates inversely with both Z_i (henceforth indicated as just *Z*) and mean K−O bond length, <K−O>, in the K micas. Inspection of Fig. 1 further reveals that the interlayer space is the most "porous" region of the mica structure. Thus, intra-unit-cell ionic porosity variations correlate with (and probably account for) the diffusional anisotropy noted above.

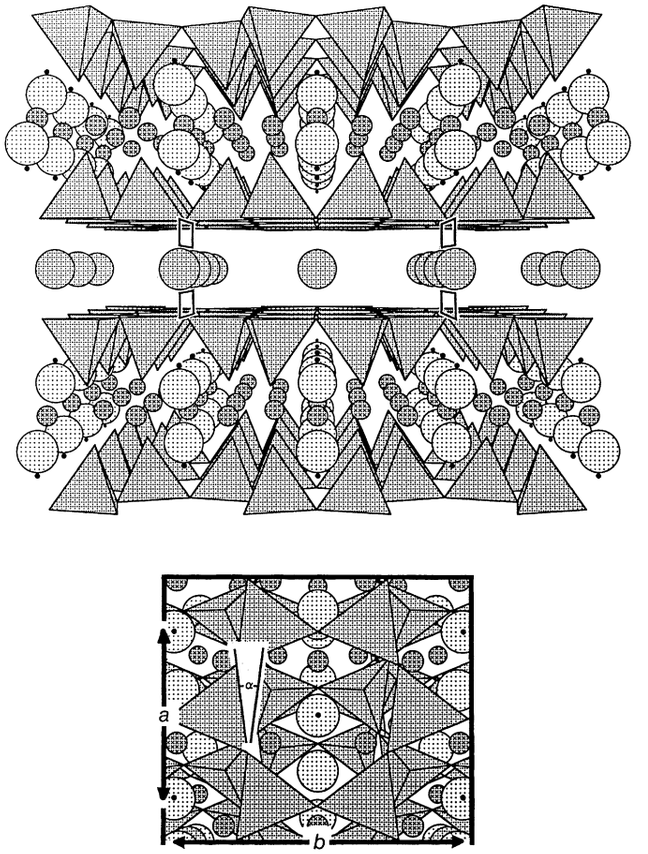

Fig. 1 The crystal structure of phlogopite, $KMg_3AlSi_3O_{10}(OH)_2$. *Perspective* view (down the *a* axis) accentuates the open, highly "porous" interlayer region of the unit cell focused upon in the text. Its volume, V_i, encloses the central K^+ and is represented by a *rectangular box* (only the *left* and *right* sides of which are drawn, for the sake of clarity); cell parameters *a*, *b*, and c_i* constitute the depth, width, and height of the box, respectively (i.e., $V_i = abc_i$*). SiO_4 tetrahedra and cations in 6-fold coordination are shown to scale [ionic radii, *r*, equal 1.38 Å for K^+ (*dense dotted pattern*) and 0.72 Å for Mg^{2+} (*cross pattern*); Shannon 1976]; radii of 1.38 Å and 0.2 Å were chosen for hydroxyl O^{2-} and H^+ (*open dotted pattern* and *solid black dots*, respectively). The structure (as refined by Hazen and Burnham 1973) was imaged using the program ATOMS for Windows (version 3.1) written by Eric Dowty, augmented with approximate hydroxyl H^+ locations of Giese (1984). In dioctahedral micas (e.g., muscovite), O−H bonds are directed into vacant M_1 octahedra sub-parallel to the T−O−T sheet, instead of sub-normal as indicated above for trioctahedral phlogopite (and biotite); see text for details. *Inset* (*perspective* view down $c \sin\beta$) shows di-trigonal tetrahedral ring enclosing the interlayer cavity (K^+ omitted for clarity); tetrahedral rotation angle, α, is also shown. *Double-arrowed* lines indicate *a*–*b* unit-cell dimensions, scaled relative to the upper hydroxyl layer

Summary of partitioning systematics

Relevant interlayer species in the micas include: (1) K^+, Rb^+, Cs^+, Ba^{2+}, Sr^{2+}, Ca^{2+}, La^{3+}, Na^+, H_3O^+, and H_2O; and (2) radiogenic $^{87}Sr^{2+}$ and ^{40}Ar, which are produced (but not necessarily housed) in the interlayer cavity.

The very fact that these chemical species do not partition randomly in interlayer sites of coexisting micas (e.g., Dahl et al. 1993; see also Table 2) indicates that these sites are energetically distinct. In fact, three specific observations about interlayer partitioning are pertinent to relative K−O bond length/strength and isotopic mass-transfer kinetics in micas. *First*, muscovite preferentially incorporates interlayer cations that are *smaller* than K^+ – namely, Na^+, Ba^{2+}, Sr^{2+}, and La^{3+} – whereas coexisting OH-biotite/phlogopite (henceforth termed biotite) favors the relatively *larger* Rb^+ and Cs^+ (e.g., see data of Volfinger 1976; Papike et al. 1984; Shearer et al. 1986; Dahl et al. 1993). *Second*, apparent interlayer vacancies are more abundant in biotite than in coexisting muscovite (e.g., see data of Rambaldi 1973; Tracy 1978; Fletcher and Greenwood 1979; Hodges and Spear 1982; Guidotti 1984; p. 407 and 446; Dutrow et al. 1986; Shearer et al. 1986; Dahl et al. 1993). *Third*, although Ba^{2+} generally favors muscovite over biotite (e.g., see data of de Albuquerque 1973, 1975; Tracy 1978; Shearer et al. 1986; Dahl et al. 1993), its partitioning actually varies system-

Table 2 Selected interlayer-element partitioning data for coexisting biotite and muscovite in F-poor compositions

Ion	K_D* (ion)	r(Å)[a]	Reference
Cs^+	6	1.67	Shearer et al. 1986
Rb^+	2.5	1.52	Shearer et al. 1986
K^+	1.0	1.38	
La^{3+}	0.8 ±0.7	1.03	Dahl et al. 1993
Ba^{2+}	0.43±0.05[b]	1.35	Dahl et al. 1993
Sr^{2+}	0.4 ±0.4	1.18	Dahl et al. 1993
Na^+	0.2 ±0.1	1.02	Dahl et al. 1993

[a] r=ionic radius for 6-fold coordination (Shannon 1976). For a given cation, $K_D^* = X_{bio}/X_{mus}$ (Dutrow et al. 1986); for K^+, a value of 1.0 is inferred from ideal mica formulas

[b] Based on 46 of the 49 mica pairs reported by Dahl et al. (1993); one of the original 49 proved to be F-rich, and two were eliminated for analytical reasons

atically with the F content in biotite – an effect previously unrecognized in the literature. Interlayer partitioning data from various sources are summarized in Tables 2 and 3, and their crystal-chemical implications are elaborated upon below.

Inferences from Rb, Cs, Na, and La partitioning

The main inference to be drawn from the correlation of interlayer partitioning and cation radius (observation no. 1 above) is that biotite possesses a relatively spacious interlayer with correspondingly large cation sites, whereas the interlayer sites of muscovite are more collapsed in the *a*–*b* crystallographic directions (Fig. 1; see also Papike et al. 1984; Shearer et al. 1986; Dahl et al. 1993). This further implies that the mean <K−O> in biotite ($<K-O>_{bio}$; averaged over the whole unit cell) exceeds that in coexisting muscovite ($<K-O>_{mus}$). Moreover, since its two unit-cell K^+ cations reside in the larger interlayer volume, it is intuitively expected that biotite possesses the higher value of *Z*. Thus, these partitioning data alone suggest that interlayer bonding in metamorphic biotite is generally weaker than in coexisting muscovite.

Crystallographic data (summarized in Table 4) support this inference. The *a*–*b* unit-cell dimensions (25° C) of muscovite are shorter than for biotite because its octahedral sheet is dominated by Al^{3+} versus the relatively larger $(Fe,Mg)^{2+}$. Thus, muscovite exhibits more *a*–*b*-plane α-rotation of adjacent tetrahedra than biotite ($\alpha \approx 11$–$13°$ versus $\sim$4–8°, respectively, at 25° C) in accommodating its tetrahedral-octahedral misfit (Bailey 1984). Moreover, these micas maintain comparable interlayer separations (c_i*, as measured along $c \sin\beta$ from the centers of opposing basal oxygen planes; see Fig. 1) unless there is substantial $F(OH)_{-1}$ component in biotite (Table 4).

Collectively, therefore, these data indicate that muscovite at room conditions has: (1) a smaller interlayer unit-cell volume, V_i (i.e., the product (abc_i*), of $\sim$158–159 Å^3 versus the $\sim$168–170 Å^3 estimated for biotite (e.g., annite in Table 4); (2) a shorter mean <K−O> than for biotite, based upon the inverse relationship between α and mean <K−O> (see also Moloshag and Teremetskaya 1975); (3) a smaller Z_i of $\sim$44.5–46.0%, versus $\sim$49% for annite (Tables 1 and 4). Interlayer porosities given in Tables 1 and 4 were calculated according to the expression:

$$Z_i(\%) = [1-(V/V_i)] \times 100\% \qquad \text{Eq. [1]},$$

where V is the total volume of interlayer ions within V_i (e.g., two K^+ and 6 O^{2-} in the ideal K mica) as determined from compositional data and ionic radii. The smaller Z_i obtained for muscovite indicates closer atomic spacings (K−K, O−O, and K−O; see Fig. 1) and implies relatively stronger K−O bonding compared to biotite. This is consistent with observations of relative resistance of muscovite to leaching, attributed in part to the fact that K^+ is especially compressed into the interlayer cavity because its large size prevents the full α-rotation dictated by tetrahedral-octahedral misfit (cf., α for paragonite with its smaller Na^+; Table 4; see also Bailey 1984 and Giese 1984).

Inferences from interlayer-vacancy partitioning

The second observation above – namely, the systematic preference of interlayer vacancies in biotite relative to muscovite – potentially also bears on relative interlayer bond strengths. The term *apparent* vacancies is actually more appropriate, given that mica interlayers can contain significant H_2O and/or H_3O^+ (Hervig and Peacock 1989; Guidotti and Dyar 1991; Dyar et al. 1991; Fortier and Giletti 1991; Loucks 1991), which are not analyzed by electron microprobe. In any case, it would seem that interlayer bonding of biotite should be weaker than that of muscovite, given its correspondingly lower abundance of (K,Na)-O bonds averaged over the unit cell in the *a*–*b* plane and the relatively low lattice binding energies of H_2O/H_3O^+ (Loucks 1991; see also Vaughan and Guggenheim 1986). As such, the *Z*-enhancing (apparent-) vacancy effect should reinforce the K−O bond-length effect described above in facilitating isotopic mass transfer in biotite – by any mechanism rate-limited by K−O bond strength (see also Loucks 1991). Indeed, the theory that vacancies (and other crystal defects not shown in Fig. 1) promote volume diffusion in minerals is well known (e.g., Lasaga 1981); more vacancies mean that fewer lattice distortions are required for an Ar atom to diffuse out to the mica surface (Villa 1991).

Inferences from Ba partitioning

The third observation cited above – namely, that Ba^{2+} favors muscovite over biotite except in F-rich compositions – underscores important contributions of O−H bond orientation and hydroxyl replacement to K−O bond

Table 3 Partitioning data for Ba and F in coexisting metasedimentary micas. Low-, intermediate-, and high-F mica data are from Dahl et al. (1993; 46 micas), Shearer et al. (1986), and Tracy (1991), respectively (samples St-5 and I-21 are from P.S. Dahl, unpublished data). Although tabulated here as biotites, Tracy's micas are actually phlogopites. Equilibrium coexistence is assumed between his micas, hence the designation "3–4" below for phlogopite 3 and muscovite 4, etc.; see text

Sample no.	Ppm Ba		X_{Ba}		Wt% F		X_F		K_D* (Ba)
	Biotite	Muscovite	Biotite	Muscovite	Biotite	Muscovite	Biotite	Muscovite	
Low-F:									
	804 ±229	2130 ±610	0.0053 ±0.0015	0.0123 ±0.0035	<0.30	<0.10	<0.04	<0.03	0.43 ±0.05
Intermediate-F:									
E2.5	1100	2300	0.0036	0.0066	0.37	0.09	0.044	0.009	0.55
E7	950	1870	0.0031	0.0054	0.34	–	0.041	–	0.57
E16A	1200	2400	0.0040	0.0069	0.34	0.10	0.041	0.010	0.58
I-21	1018	1500	0.0034	0.0043	1.18	0.44	0.141	0.045	0.79
E4	900	1300	0.0030	0.0037	0.41	–	0.049	–	0.81
E3	920	1460	0.0030	0.0042	0.66	0.13	0.079	0.013	0.71
E12	850	1600	0.0028	0.0046	0.43	0.14	0.052	0.014	0.61
St-5	748	1490	0.0025	0.0042	0.63	0.21	0.076	0.026	0.60
Mean					0.55 ±0.29		0.07 ±0.03		0.65 ±0.09
High-F:									
3–4	28800	21700	0.0900	0.0660	2.86	0.32	0.325	0.036	1.36
1–4	25800	21700	0.0800	0.0660	2.87	0.32	0.323	0.036	1.21
3–6	28800	25200	0.0900	0.0760	2.86	0.32	0.325	0.035	1.18
1–6	25800	25200	0.0800	0.0760	2.87	0.32	0.323	0.035	1.05
Mean					2.87		0.32		1.20 ±0.11

strength in coexisting micas. The crystal-chemical connection between Ba^{2+} partitioning, hydroxyl orientation, (F,Cl,O)-content, and relative K−O bond strength in coexisting micas is now developed.

The partitioning behavior of Ba^{2+} diverges markedly from that of K^+ in metapelitic compositions (Dahl et al. 1993) despite their comparable ionic radii (r^{vi-xii}=1.35–1.61 Å and 1.38–1.64 Å, respectively; Shannon 1976). This raises a fundamental question: why does a large cation like Ba^{2+} (which follows K^+ crystallochemically; Harlow 1991) strongly prefer the laterally collapsed interlayer sites in muscovite (see Tables 2 and 4), despite the availability of seemingly more favorable (i.e., larger, less α-rotated) sites in coexisting biotite? Indeed, no suitable explanation for this apparent anomaly is found in the literature, beyond speculation that separate Ba-related charge-balance mechanisms operating simultaneously in muscovite and biotite somehow favor muscovite (Dahl et al. 1993). For micas generally, Harlow (in press) emphasized the roles of charge-balance and interlayer geometry (as dictated by the degree of α-rotation) in governing Ba^{2+} substitution. Both are enhanced by chemical substitutions [such as ^{vi}(Cr, V, Mg)Al_{-1}] that improve tetrahedral-octahedral fit so as to give a more open (i.e., less α-rotated) interlayer site, as indicated by occurrences of barian-chromian-magnesian muscovite (e.g., Dymek 1983; Tracy 1991). Likewise, Cruciani and Zanazzi (1994) have argued that Ba^{2+} substitution in synthetic phlogopite is promoted by opening of its interlayer cavity by Ti-oxy-mica substitution; this effect may also account for extreme Ba enrichment observed in some natural biotite/phlogopites (e.g., Wendlandt 1977; Mansker et al. 1979).

The size argument outlined above still does not explain why Ba^{2+} typically prefers the small interlayer sites of metapelitic muscovite over the larger such sites in biotite. It is suggested here that Ba^{2+} partitioning between muscovite and OH-biotite is governed largely by the differing hydroxyl orientations in the two micas. It has long been known that O−H bonds are oriented sub-*normal* to the (001) plane in trioctahedral micas (Fig. 1) and sub-*parallel* to this plane in dioctahedral micas (Serratosa and Bradley 1958; Giese 1979, 1984). Moreover, covalency of the O−H bond effectively means that a bare proton is projected into the interlayer cavity of biotite (Giese 1984). Thus, it is postulated here that repulsion by H^+ directed into the interlayer cavities from adjoining T−O−T sheets causes an overriding electrostatic destabilization of Ba^{2+}, despite: (1) the excellent size suitability of biotite interlayer sites for Ba^{2+} substitution, and (2) the small size and low abundance of H^+. Moreover, judging from formal ionic charges, Ba^{2+} should experience approximately twice the Coulombic repulsion of K^+ in biotite. Corollary to this hypothesis, the interlayer sites of muscovite (despite their small size) are electrostatically more *conducive* to Ba^{2+} substitution because potential repulsion by the proton is minimized by virtue of the O−H bond being directed into the vacant *M*1 octahedron, sub-parallel to the (001) plane. The net result is that Ba^{2+} strongly prefers muscovite over biotite, as indi-

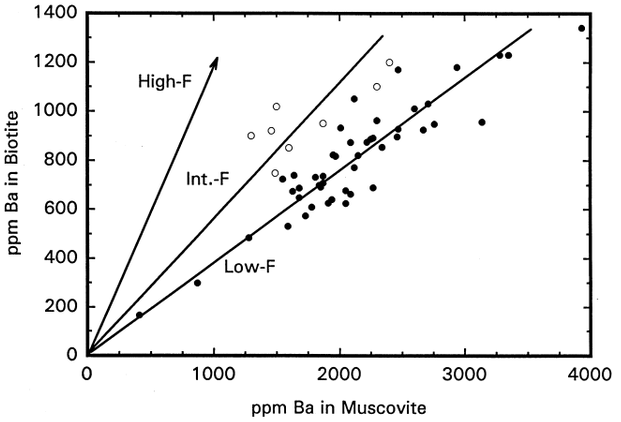

Fig. 2 Distribution diagram for Ba between coexisting biotite and muscovite in metasedimentary rocks from the southern Black Hills, SD. *Solid circles* represent 46 *low*-F, staurolite- and sillimanite-zone mica pairs from Dahl et al. (1993); F analyses are from P.S. Dahl (unpublished data). *Open circles* represent eight *intermediate*-F mica pairs in schists adjacent to rare-alkali pegmatites; six rocks are from Shearer et al. (1986), one is from Dahl et al. (1993; sample St-5), and one is from P.S. Dahl (sample I-21, unpublished data). Regression lines (forced through the origin) are shown for the two datasets, which differ significantly at the 1σ level. A third line trends toward four *high*-F phlogopite-muscovite "pairs" of Tracy (1991), which actually plot well beyond the scale of the diagram. All lines are labeled with corresponding ranges of wt% F in biotite/phlogopite (see Tables 2 and 3 for data summaries)

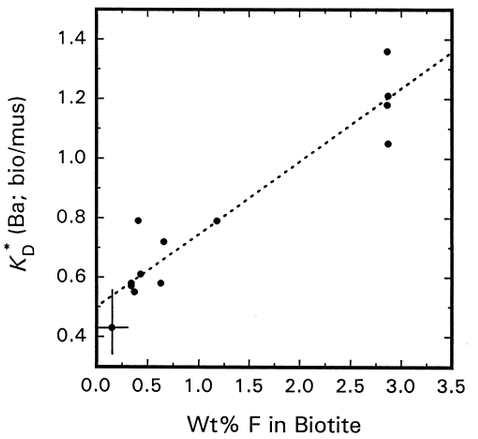

Fig. 3 Plot of K_D* (Ba;biotite/muscovite) versus wt% F in biotite. The 46 low-F mica pairs from Dahl et al. (1993) are represented by the *cross*, which brackets K_D* and wt% F (biotite) for the dataset. The intermediate- and high-F data plotted are from Shearer et al. (1986) and Tracy (1991), respectively, as summarized in Table 3

cated in selected data for metapelites (Table 3), plus other data from the literature (cited above).

An effective test of the hydroxyl-orientation hypothesis would be verification that *removal* of hydroxyl H^+ in biotite renders its interlayer sites *more competitive* for Ba^{2+} substitution. Removal of the proton and concomitant elimination of K^+-H^+ or $Ba^{2+}-H^+$ repulsion are effected in biotite/phlogopite by $(F,Cl,O)(OH)_{-1}$ exchange, as evidenced by reduced interlayer separations (i.e., contraction along $c\sin\beta$) in: (1) F-phlogopites relative to OH-phlogopites (Yoder and Eugster 1954), and (2) oxy-biotites relative to hydrogenated oxy-biotites and biotites (Ohta et al. 1982; Bailey 1984). Electrostatically, therefore, $(F,Cl,O)(OH)_{-1}$ exchange ought to encourage Ba^{2+} substitution in biotite/phlogopite. In contrast, this exchange vector in coexisting muscovite ought to be relatively inconsequential vis-à-vis Ba^{2+} substitution because: (1) muscovite has relatively low halogen abundances (Evans 1969; Munoz and Ludington 1977; Nemec 1980; Shearer et al. 1986; Tracy 1991), and (2) its hydroxyls are oriented sub-parallel to (001), such that electrostatic repulsions involving the interlayer are small to begin with. Therefore, the overall expectation is that progressive $(F,Cl,O)(OH)_{-1}$ exchange in coexisting micas should cause corresponding increase in the value of K_D* (Ba;bio/mus) – defined here as $X_{Ba}^{bio}/X_{Ba}^{mus}$ (following Dutrow et al. 1986), where X_{Ba} denotes mole fraction of Ba in the interlayer sites of biotite (or phlogopite) and muscovite.

Indeed, the predicted partitioning behavior is actually observed in the limited Ba−F data currently available for coexisting muscovite and biotite (Table 3; Figs. 2–3). Figure 2 illustrates Ba distributions for three coexisting mica datasets distinguished by their mean F-content in biotite, and Fig. 3 shows the positive covariance of K_D* (Ba) and wt% F. *High*-F, Ba-phlogopites (F=2.9 wt%) and Ba−Cr−Mg-muscovites from veins in marble at Franklin, NJ (Tracy 1991) plot far off-scale in Fig. 2 but nominally partition Ba almost randomly [K_D* (Ba;phl/mus)$=1.20\pm0.11$]; F-saturation of vein micas is indicated by the presence of fluorite. In contrast, *intermediate*-F biotites [$F=0.55\pm0.29(1\sigma)$ wt%] from 8 metapelites adjacent to Li-B-F-rich intrusive pegmatites in the Black Hills, S.D. (Shearer et al. 1986; P.S. Dahl, unpublished microprobe data) exclude Ba relative to coexisting muscovites. [K_D* (Ba;bio/mus) $=0.65\pm0.09(1\sigma)$]. Also low-F biotites ($F\leq0.3$ wt%) from 46 rocks sampled beyond these metasomatic pegmatite haloes (Dahl et al. 1993; P.S. Dahl, unpublished microprobe data) exclude Ba even *more* [i.e., K_D* (Ba;bio/mus)$=0.43\pm0.05(1\sigma)$]. These low-F micas are typical of average metapelites elsewhere (i.e., $F\leq0.3$ wt%; Guidotti 1984, p. 428). A close approach to partition equilibrium in the low-F dataset is indicated by its linearity and close approach to the origin (Fig. 2), and the inferred K_D* (bio/mus) difference between it and the *intermediate*-F dataset is significant at the 1σ level. Partition equilibrium is assumed here for the high-F micas of Tracy (1991), which occur as small isolated flakes in the veins. Moreover, it is assumed that Henry-ion behavior of Ba^{2+} extends also to Tracy's micas ($X_{Ba}=0.07$–0.09).

In advancing a cause-and-effect relationship between K_D* (Ba) and wt% F in biotite/phlogopite, it is important to rule out significant effects by other compositional

variables. Besides the differences in Ba and F abundance noted above (see Table 3), the other main differences among the datasets lie in the relative Mg enrichment and Ti depletion of Tracy's (1991) phlogopites compared to the Black Hills biotites. Also, Tracy's muscovites are more Mg- and Cr-rich than the Black Hills muscovites. The main effect of relatively high $MgFe_{-1}$ substitution in a biotite/phlogopite is to increase α-rotation (Circone et al. 1991), which inhibits Ba^{2+} substitution (Cruciani and Zanazzi 1994). Likewise, low-Ti abundances in Tracy's (1991) phlogopites suggest limited Ti-oxy-mica substitution and a correspondingly limited encouragement of Ba^{2+} substitution (Cruciani and Zanazzi 1994). Finally, the enhanced Mg and Cr substitutions in Tracy's muscovites serve to enlarge the octahedral strip and interlayer sites (by reducing α), which will enhance Ba^{2+} substitution in muscovite (Cruciani and Zanazzi 1994). If any or all of these effects exerted dominant control on K_D* (Ba), then we would expect the mica "pairs" of Tracy (1991) to yield lower K_D* values than the Black Hills mica pairs. Because just the opposite relative K_D* relationship is actually observed, however, it is concluded that some other compositional effect exerts overriding control on K_D*. This leaves only F-content to account for the observed K_D* differences documented in Table 3, as we have suggested preference above.

In summary, the unequivocal preference of Ba^{2+} for muscovite over OH-biotite in metapelites (Tables 2–3; Figs. 2–3) is largely attributed to known differences in hydroxyl orientations of the two micas (although competing charge-balance reactions may also be involved). Supporting this hypothesis are preliminary data indicating that $F(OH)_{-1}$ exchange increases the value of K_D* (Ba) (see Figs. 2–3; Table 3). Further support comes from a crystal-chemical study of phlogopite by Cruciani and Zanazzi (1994). In documenting a parallel increase in Ba^{2+} and Ti-oxy-mica substitution in phlogopite, they attributed the entry of Ba^{2+} to both decreased interlayer repulsion arising from progressive proton removal by $O(OH)_{-1}$ exchange and the interlayer-cavity opening discussed earlier. Insufficient data preclude inference of a K_D* (Ba)-O trend parallel to the K_D* (Ba)-F trend shown in Fig. 3, but the existence of such a trend is highly likely.

The fundamental kinetic inference from differing hydroxyl orientations in coexisting micas is that net K−O bond strength in muscovite exceeds that in OH-biotite, because of relatively less K^+-H^+ repulsion (see also Guggenheim et al. 1987). The interplay of hydroxyl orientation and K−O bond strength was first suggested by Bassett (1960) in a weatherability study of micas. Inverting Bassett's argument, progressive $F(OH)_{-1}$ substitution in trioctahedral micas should concomitantly *strengthen* interlayer bonds to K^+; parallel arguments follow for $Cl(OH)_{-1}$ and $O(OH)_{-1}$ (oxy-mica) substitutions. Indeed, synthetic fluorphlogopite possesses much greater thermal stability than phlogopite (Deer et al. 1963), and oxy-annite has a higher thermal stability than annite (Wones 1963).

Summary

Independent confirmation of the relative bond strengths postulated above for the common micas is provided by quantitative electrostatic modeling. *First,* Pauling K−O strengths (z/p, where z is the charge of the cation and p is its coordination number) may be higher for muscovite because its effective coordination number is somewhat lower (due to higher α). *Second,* Giese (1984) found the electrostatic energies required to separate adjoining T−O−T sheets to their normal 3.3–3.4 Å spacing in these micas to be 28 kcal/mole ($2M_1$ muscovite) and 15 kcal/mole ($1M$ OH-phlogopite). An intermediate value of ~20 kcal/mole for $1M$ F-phlogopite probably reflects strengthening of the K−O bond (by $F(OH)_{-1}$ substitution in OH-phlogopite. Indeed, this substitution causes interlayer collapse along $c\sin\beta$ (Yoder and Eugster 1954) which is manifested as a reduction of Z at room conditions (cf., OH- and F-rich phlogopites in Table 4). *Third,* FIR spectroscopic studies (Larsen et al. 1972) show higher-energy infrared absorption for muscovite than for biotite (i.e., peaks at 105 cm^{-1} versus 85 cm^{-1}, and at 160 cm^{-1} versus 140 cm^{-1}), suggesting a stronger K−O bond in muscovite.

Differential kinetic responses of coexisting micas to various processes: natural and experimental observations

The relatively lower K−O bond strength inferred above for biotite (high Z) versus muscovite (lower Z) increases the probability of bond stretching, compression, or breakage – in other words, lowers the activation energy barriers to transformation generally. In fact, K−O bond strength appears to be the common thread on which can be hung the differential kinetic responses of coexisting micas to a host of otherwise unrelated processes – many of which are important to geochronology. Supporting this view are observations that OH-biotite is consistently more susceptible than muscovite to:

1. Diagenetic alteration and K loss during weathering (Bassett 1960; Farmer et al. 1971; Norrish 1973; Boles and Johnson 1983; Clauer 1981; Mitchell and Taka 1984; Mitchell et al. 1988; Lo and Onstott 1989; Kelley and Bluck 1992), although petrologic factors are as important if not more so;
2. Deformation, fluid-mediated dissolution/neocrystallization, and solid-state recrystallization in nature (Wilson and Bell 1979; Meike 1989);
3. Argon release, weight loss, and delamination during *in vacuo,* incremental step-heating experiments (Zimmermann 1970; Gaber et al. 1988);
4. Loss of O and Ar in hydrothermal bomb experiments, particularly in the lower temperature range (Robbins 1972; Harrison et al. 1985; Fortier and Giletti 1991);
5. Argon loss in nature, generally promoting younger cooling ages in metamorphic rocks (McDougall and Har-

rison 1988; Hodges et al. 1994) and younger thermally reset ages (Villa and Puxeddu 1994); and
6. Incorporation of excess Ar in nature (see Brewer 1969, and references contained therein), either by diffusion or recrystallization mechanisms (Dallmeyer and Gee 1986).

Parallel compositional effects on kinetics are commonly evident within the trioctahedral and dioctahedral subgroups, Mg- and/or F-rich varieties being among the more resistant to transformation. The variable kinetic behavior of micas to the above-listed processes and effects on age are now explored in greater detail.

Processes (1)–(3): alteration, deformation, and recrystallization (mineralogical and microstructural)

The greater weatherability of trioctahedral micas relative to their dioctahedral counterparts is well known, as is the related fact that biotites release K (and Ar) to soils more readily than muscovites (Bassett 1960; Farmer et al. 1971; Norrish 1973). These authors advanced the OH-orientation argument outlined above to suggest that K is more weakly held in biotite during weathering. The validity of this argument is buttressed by the fact that F-phlogopite is more resistant to weathering than OH-phlogopite (Deer et al. 1963).

Boles and Johnson (1983) also suggested that weakly held K^+ in biotite accounts for its preferential diagenetic alteration relative to muscovite (without giving a crystal-chemical reason, however). Specifically, they showed that sheared/crushed biotite readily exchanges K^+ with pore water H^+, thus lowering local pH and promoting growth of diagenetic carbonate minerals and OH-bearing phases (like laumontite, prehnite, and epidote) in (001) cleavage planes. In addition, biotite seems more prone than muscovite to *hydrothermal* alteration, judging from its tendency to become chloritized. The crystal-chemical controls on K−O bond strength (developed above) potentially explain this differential behavior too, although not necessarily to the exclusion of petrologic effects.

In deformational environments at given $P-T$ conditions, the kinetics of deformation, dissolution, nucleation, and (re)crystallization appear to be more favorable in biotite than in muscovite – according to detailed textural analysis of metamorphic tectonites by Wilson and Bell (1979). They found that biotite was intensely folded or kinked, whereas the more competent muscovite in the same rock generated only sinusoidal folds. Moreover, they noted enhanced fluid-mediated dissolution of deformed biotite and crystallization of new biotite, as evidenced by irregular grain boundaries and serrated fracture planes with new overgrowths, etc.. Coexisting muscovite, on the other hand, lacked evidence of these features. Wilson and Bell also inferred greater susceptibility of biotite to solid-state recrystallization, based upon the observation of small, segmented, sub-grains in larger biotite grains; again, coexisting muscovite lacked such sub-grains (see also Meike 1989). Finally, Vernon (1977) documented kink-related dilatation zones in biotite, associated with deformation-enhanced loss of cohesion across the (001) plane, but did not report such dilatation in coexisting muscovite. This apparent difference is consistent with *in vacuo* incremental heating experiments (Zimmerman 1970; Gaber et al. 1988) showing that biotite delamination along (001) occurs more readily (i.e., at lower temperature) than in muscovite, accompanied also by earlier water/argon loss and overall weight loss. Neither Wilson and Bell (1979) nor Vernon (1977) presented a crystal-chemical explanation for their observations. Collectively, however, their observations – plus those of Zimmerman (1970) and Gaber et al. (1988) – are fully consistent with the hypothesis that K^+ is held more weakly in biotite than in muscovite, as postulated here from K_D* and Z considerations.

At first glance, kinetic data for basal-plane dislocation glide in muscovite and biotite (Mares and Kronenberg 1993; Kronenberg et al. 1990) appear to contradict this hypothesis. These workers experimentally documented that muscovite was actually *weaker* than biotite, a result they themselves did not anticipate, presumably because it contradicted the detailed textural observations of Wilson and Bell (1979). However, it is noted here (see also Dahl and Dorais, in press) that the biotite deformed by Kronenberg et al. (1990) *was actually an F-rich phlogopitic mica.* Recalling from the crystal-chemical framework developed above that $F(OH)_{-1}$ substitution in trioctahedral micas *strengthens* interlayer bonds to K^+, it follows that the kinetics of dislocation glide should be correspondingly *inhibited* in an F-rich mica. The inference that such a mica could thus be stronger than muscovite is supported by the independent observation that volume diffusion is *also* inhibited in F-rich phlogopite relative to muscovite (see Table 1). Moreover, biotite delaminates at lower temperature than phlogopite during *in vacuo* step-heating experiments (Zimmermann 1970; T.C. Onstott, personal communication to Gaber et al. 1988), which probably reflects the kinetic response to lower abundance of $MgFe_{-1}$ and/or $F(OH)_{-1}$ components.

The kinetic/geochronologic prediction from the textures and experiments described above is preferential isotopic rejuvenation and younger ages in metamorphic OH-biotite in rocks where biotite and muscovite (of equal grain size) were subject to the same deformational and fluid regime – either above or below nominal closure temperatures, T_c(Ar). Indeed, this prediction is typically fulfilled in dating projects (McDougall and Harrison 1988), and by mechanisms as outlined below. (A corollary prediction that OH-biotites should be rejuvenated more readily than their F-rich counterparts has not yet been isolated in geochronologic studies, however).

Above nominal T_c (>350° C), incipient retrograde deformation will result in more strain dislocations (bounding kinked sub-grains) in OH-biotite than in the more competent muscovite; in other words, biotite will recrystallize more readily. Barring subsequent annealing, selective recrystallization of biotite into smaller sub-grains reduces its effective diffusion dimension [and T_c in the

Dodson (1973, 1986) equations; e.g., Goodwin and Renne 1991], promoting preservation of the younger cooling age in biotite relative to coexisting muscovite – all other factors equal. Preferential alteration (i.e., chloritization) of OH-biotite, mediated by fluids, reinforces this effect by likewise partitioning the biotite into sub-grain argon diffusion domains (e.g., Lo 1988). Moreover, these processes may be intimately interrelated; fluid infiltration often accompanies deformation, and alteration phases commonly exploit crystal defects (Veblen 1980; Brodie and Rutter 1985; Walther and Wood 1986).

Below nominal T_c, differential rejuvenation of micas may be facilitated by incipient, deformation/fluid-induced dissolution/neocrystallization – producing younger apparent ages in direct proportion to the mineral volume transformed (cf., the intermediate plateau age obtained by Berry and McDougall 1986, for a mixed population of relict, retrogressed, and new hornblende). Thus, even if $^{40}Ar/^{40}K$ ratios and closure ages of muscovite and biotite were initially *identical* (say, from earlier fast cooling in a pluton), biotite should still yield the younger plateau age (representing a mix of old and new generations), since it potentially incurs the larger volume-percent transformation in response to incipient, sub-closure deformation or fluid infiltration. Of course, *complete* transformation of *both* micas in a rock will accompany *pervasive* deformation or fluid infiltration, resulting in concordant regrowth ages (as also documented for hornblende; Berry and McDougall 1986).

The hypothesis that ages preserved in micas reflect rates (progress) of recrystallization and alteration is supported by relative $^{40}Ar/^{39}Ar$ ages of progressively transformed hornblendes in adjacent rocks (Berry and McDougall 1986; Onstott and Peacock 1987), in which the Fe-rich, more transformed varieties (and nominally higher *Z*; Dahl in press) yield the younger ages.

Processes (4)–(6): volume diffusion (experimental and natural)

Experimental micas

Volume diffusion will dominate ^{40}Ar retention properties in micas in high-grade terranes slowly cooled under relatively "dry" and static conditions, since the catalysts to drive reaction and/or recrystallization processes are largely absent (i.e., fluids and deformation). Moreover, volume diffusion may govern argon loss and gain by these minerals during reheating events and exposure to non-zero argon pressures, respectively. Just as with recrystallization and reaction, the kinetics of ^{40}Ar volume diffusion are *also* potentially linked to electrostatic and repulsive forces between bonded ions in crystal structures (Lasaga 1981; Voltaggio 1985). The evidence for such relationships in micas is developed and systematized below.

Fortier and Giletti (1991) reported that O diffusivities among muscovite, biotite, and F-rich phlogopite differ by only a factor of two (i.e., within analytical uncertainty) at 700° C, and concluded that diffusivity-composition ($D-X$) effects are minor at this temperature. However, at the 500° C end of their experimental range, this difference nominally increases to a factor of eight – with $D_{bio} > D_{mus} > D_{F\text{-}rich\ phl}$ (Table 1) – and is magnified yet *further* upon extrapolation to the nominal 300–400° C range of mean closure temperatures for micas (see Figs. 7–8 of Fortier and Giletti 1991). A parallel diffusivity trend for ^{40}Ar also exists (Table 1), although the data for muscovite are relatively unconstrained (McDougall and Harrison 1988; Hames and Bowring 1994). We may now conclude from crystal chemistry that relatively strong K−O bonds in experimental muscovite and F-rich phlogopite (Robbins 1972; Giletti 1974a; Fortier and Giletti 1991) account for their lower D values compared to those obtained for F-poor biotite (Harrison et al. 1985; Fortier and Giletti 1991). Recent diffusion experiments (Grove and Harrison 1993, 1994) have confirmed the $F(OH)_{-1}$ effect on argon diffusivity within the trioctahedral micas. Moreover, Grove and Harrison (1994) explicitly invoke the same K^+-H^+ repulsion argument to explain their data as independently invoked here to rationalize the Ba^{2+} partitioning data. In fact, this mutual appeal to a common crystal-chemical effect affirms the prior suggestion of Dahl et al. (1993; see also Introduction) that isotopic mass-transfer kinetics and element partitioning behavior are both governed by the same aspects of interlayer crystal chemistry.

Natural micas

The relative ^{40}Ar diffusivities of OH-biotite and muscovite (Table 1) are inversely correlated with $^{40}Ar/^{39}Ar$ cooling age, as evidenced by the age-zoned micas of Hodges et al. (1994). Hodges et al. convincingly documented differential diffusive-loss profiles for argon in very slowly cooled single crystals of muscovite (slow diffuser) and younger coexisting biotite (fast diffuser). Elsewhere, the relative ^{40}Ar diffusivities of OH-biotite and muscovite are also consistent with the observed tendency for metamorphic biotite preferentially to: (1) reset isotopically during reheating events, and (2) incorporate excess argon.

An excellent example of preferential resetting is young, *Alpine*-reset biotite coexisting with older *Hercynian* muscovite, as documented in a recent study by Villa and Puxeddu (1994). Isotopic resetting progress was quantified by Dodson (1975) in terms of duration/intensity of the thermal pulse and magnitude of the diffusion parameters (E and D_o). His equation predicts relatively enhanced thermal resetting of biotite (lower E; see above) and the corollary observation that biotite preserves younger ages upon reheating.

The classic proof of preferential excess-argon incorporation in biotite is the work of Brewer (1969). He showed by parallel K−Ar and Rb/Sr dating that the K−Ar "ages" in biotites (compared to ages in coexisting muscovites) were anomalously high, a phenomenon also

observed by subsequent workers in the $^{40}Ar/^{39}Ar$ system (see McDougall and Harrison 1988). Diffusional and recrystallization mechanisms for incorporation of excess argon are evident (Foland 1983; Reddy et al. 1995; Arnaud and Kelley 1995), but both are kinetically favored in biotite. Therefore, irrespective of which process occurred during an interval of exposure to high partial pressure of ^{40}Ar, biotite will tend to incorporate more ^{40}Ar into its crystal structure until or unless the process has gone to completion in both micas. Preservation of this relative excess requires only that the micas must have cooled through their closure interval before the high partial pressure of ^{40}Ar had time to dissipate (Brewer 1969). In contrast, if both micas incorporated excess argon uniformly, porosity considerations predict that the white mica (low Z) will preferentially retain its excess compared to biotite (higher Z) where cooling through closure was synchronous with or later than dissipation of the excess partial pressure. Indeed, this is how Arnaud and Kelley (1995) explained retention of a higher (and unequivocal) excess component in phengite ($Z \approx 45.5\%$, this study) relative to biotite ($Z \approx 47$–49%; i.e., a faster diffuser of Ar) in an undeformed metagranite from the Dora Maira locality, western Italian Alps. Thus, we see from these examples that porosity considerations potentially constrain the relative timing of excess Ar dissipation and closure in two-mica systems.

Geochronologic implications

Age-retentivity-composition relationships within the trioctahedral and dioctahedral mica sub-groups

The wide compositional diversity among the true-mica sub-groups in nature (Guidotti 1984) – together with various *D-X* relationships observed therein (Giletti 1974a; Harrison et al. 1985; Grove and Harrison 1993, 1994) – arouse suspicions of corresponding age-retention-composition relationships among diverse micas in adjacent lithologies (e.g., see Onstott et al. 1989). These suspicions are heightened by the likelihood that K−O bond strength is the "kinetic common denominator" for argon loss both in the laboratory and in nature.

Extension of the kinetics-porosity framework developed above for distinguishing "average" biotite ($Z \approx 47$–49%) from "average" muscovite ($Z \approx 44.5$–46%) leads us to prediction of secondary age-retention-composition relationships among both trioctahedral and dioctahedral mica solid solutions. Various age-composition predictions (and available supporting evidence) are presented below.

Trioctahedral micas (biotites and phlogopites)

Taken at face value, interlayer-porosity considerations (Table 4) predict that Ar loss in nature is variably inhibited by many of the common substitutions, including:

(1) $Mg\ Fe_{-1}$;

(2) $Al^{vi}Al^{iv}\ (Mg,Fe)_{-1}\ Si_{-1}$ (Al-Tschermak substitution);

(3) $(F,Cl)\,(OH)_{-1}$;

(4) $Ti^{4+}\square^{vi}\ R^{2+}{}_{-2}$ (R^{2+}=Fe,Mg);

(5) $Ti^{4+}\ (O^{2-})_2(H_2)\ R^{2+}{}_{-1}(OH)_{-2}$ (Ti-oxy-mica substitution);

(6) $R^{3+}\ (O^{2-})(H_2)_{0.5}\ R^{2+}{}_{-1}(OH)_{-1}$ (oxy-mica substitution; R^{3+} designates Fe^{3+} or Al^{3+}); and

(7) $(K,Na)\square_{-1}$.

These substitutions are all written in the direction of Z reduction – which itself reflects either decreased dimensions [a, b, c_i*; (1)–(6) above], or increased interlayer-cation concentration [(7) above]. According to the model, therefore, each of these substitutions promotes preservation of older $^{40}Ar/^{39}Ar$ ages in slowly cooled ($\leq 2°$ C/Ma) terranes. Thus, Z calculations and estimates (Table 4) lead to the following predictions of relative age among binary end members within the ideal trioctahedral mica plane (Guidotti 1984) – and its extension to F,Cl,O-rich compositions – in a slowly cooled (or reheated) terrane:

1. F-phlogopite (Z=45.8%) > phlogopite ($Z \approx 47.6\%$),

2. Phlogopite ($\sim 47.6\%$) > annite (49.1%),

3. Siderophyllite ($\sim 47.8\%$) > annite (49.1%)

4. "Eastonite" ($\sim 46.3\%$) > phlogopite ($\sim 47.6\%$), and

5. Oxy-biotite (47.3%) > oxy-biotite, hydrogenated (48.2%),

where Z for phlogopite, siderophyllite, and "eastonite" end members can only be estimated since requisite c_i* data are unavailable from most crystallographic studies (Yoder and Eugster 1954; Hewitt and Wones 1975; Circone et al. 1991). All other quoted Z values are considered accurate to within $\pm 0.3\%$ (absolute), so the differences inferred above are significant at the 1σ level. Nominally, the Z data indicate that $(F,Cl,O)\,(OH)_{-1}$ substitutions are as important (if not more so) than $MgFe_{-1}$ substitution in determining isotopic retention of biotite-phlogopites – as suggested also by Grove and Harrison (1993, 1994) from their Ar diffusion experiments, and in relatively inhibited Ar diffusivity documented for an F-rich phlogopite (Giletti 1974a). The influence of $MgFe_{-1}$ substitution on retention (observed by many authors) is supported by the positive correlation of infrared K vibrational frequency (i.e., K−O bond energy and strength) and Mg-content in micas generally (Laperche 1991, quoted in Scaillet et al. 1992). More important, however, is the point that modeling retention in complex multi-component solid solutions like the biotite-phlogopites cannot be restricted to any one component. Instead, Z potentially represents the broader, more appropriate compositional monitor with which to pursue modeling, in that it accounts for the crystal-chemical effects not only of $F(OH)_{-1}$ and $MgFe_{-1}$ but also those of the other

Table 4 Summary of crystal-chemical data for selected micas from the literature. (*mus* muscovite, *phe* phengite, *prg* paragonite, *mar* margarite, *phl* phlogopite, *bio* biotite, *ann* annite). Compositions are reported as ions per 11 oxygens; total Fe is reported as Fe^{2+} unless Fe^{3+} data are available from original sources. Minor Li, Cl, and H_3O^+ abundances are omitted from some analyses; F omissions are designated by **. Species not analyzed are designated by –; *N.A.* means data are not available. Calculations of V, V_i, and Z_i are from this study (see Eq. [1] and text); all other data are compiled from the literature. [*References: A* Comodi and Zanazzi (1995), *B* Guggenheim et al. (1987), *C* Güven (1971), *D* Burnham and Radoslovich (1964), *E* Lin and Bailey (1984), *F* Joswig et al. (1983), *G* Takeda and Morosin (1975), c_i* inferred (this study), *H* Ohta et al. (1982), *I* Bohlen et al. (1980); *J* Hazen and Burnham (1973)

	Dioctahedral micas (2 M_1)													
Ions per 11 oxygens:	Mus		Mus		Mus		Mus	Phe	Na-mus		Na-mus	K-prg	Prg	Mar
Na	0.07	0.07	0.03	0.03	0.08	0.08	0.10	0.07	0.37	0.37	0.34	0.85	0.92	0.21
K	0.90	0.90	1.00	1.00	0.93	0.93	0.86	0.87	0.60	0.60	0.66	0.15	0.04	–
Ca	–	–	0.01	0.01	0.01	0.01	–	0.03	–	–	–	–	0.02	0.73
Ba	0.01	0.01	–	–	–	–	–	–	–	–	–	–	–	–
Fe^{2+}	0.07	0.07	0.01	0.01	0.16	0.16	0.05	0.09	0.10	0.10	–	–	0.03	0.03
Mg	0.04	0.04	0.01	0.01	0.01	0.01	0.06	0.50	0.06	0.06	–	–	0.01	0.22
Al^{vi}	1.84	1.84	1.93	1.93	1.83	1.83	1.90	1.43	1.84	1.84	2.00	2.00	1.99	1.96
Fe^{3+}	–	–	–	–	–	–	0.02	0.05	–	–	–	–	–	–
Mn	–	–	0.01	0.01	0.01	0.01	–	–	–	–	–	–	–	–
Ti	0.04	0.04	–	–	–	–	0.01	0.01	0.02	0.02	–	–	–	–
Al^{iv}	0.98	0.98	0.91	0.91	0.90	0.90	0.98	0.61	0.97	0.97	1.00	1.00	1.06	2.08
Si	3.02	3.02	3.09	3.09	3.10	3.10	3.02	3.39	3.02	3.02	3.00	3.00	2.94	1.92
O	10.00	10.00	10.00	10.00	10.00	10.00	10.00	10.08	10.00	10.00	10.00	10.00	10.00	10.00
OH	2.00	2.00	2.00	2.00	2.00	2.00	1.99	1.92	2.00	2.00	2.00	2.00	2.00	2.12
F	–	–	**	**	**	**	0.01	–	–	–	–	–	–	–
Unit-cell data:														
a (Å)	5.151	5.194	5.158	5.182	5.200	5.215	5.191	5.211	5.130	5.165	5.174	5.134	5.128	5.110
b (Å)	8.931	9.013	8.905	9.883	9.021	9.053	9.008	9.038	8.886	8.964	8.976	8.907	8.898	8.800
c_i* (Å)	3.128	3.375	3.436	3.491	3.386	3.418	3.392	3.359	3.050	3.324	3.312	3.078	3.053	2.874
β (°)	95.8	95.8	95.8	95.8	95.7	95.7	95.8	95.8	95.5	95.4	95.6	94.6	94.4	95.0
α (°)	11.9	10.3	11.8	9.8	11.3	10.3	11.4	6.0	13.7	10.9	12.8	15.9	16.2	20.9
V (Å^3)	86.69	86.69	88.42	88.42	87.32	87.32	85.87	86.08	82.55	82.55	83.60	76.91	75.28	74.03
V_i (Å^3)	143.90	158.00	157.82	162.69	158.83	161.37	158.60	158.21	139.03	153.90	153.82	140.75	139.31	129.24
Z_i (%)	39.75	45.13	43.98	45.65	45.02	45.89	45.85	45.59	40.63	46.36	45.65	45.36	45.96	42.72
P (bars)	28000	500	1	1	1	1	1	1	27000	1	1	1	1	1
T (°C)	25	25	20	525	20	300	25	25	25	25	25	25	25	25
Reference	A	A	B	B	B	B	C	C	A	A	D	D	E	F

Table 4 (continued)

	Trioctahedral micas (1 *M*)								
Ions per 11 oxygens:	F-phl				O-bio	O-bio	Bio	FOH-phl	Ann
Na	0.04	0.04	0.04	0.04	0.16	0.16	0.02	0.16	0.07
K	0.98	0.98	0.98	0.98	0.77	0.77	0.99	0.76	0.88
Ca	–	–	–	–	–	–	–	–	0.04
Ba	–	–	–	–	0.02	0.02	–	0.05	–
Fe^{2+}	–	–	–	–	0.01	0.01	1.39	0.01	2.22
Mg	2.97	2.97	2.97	2.97	1.67	1.67	1.16	2.98	0.12
Al^{vi}	–	–	–	–	0.16	0.16	0.12	–	0.09
Fe^{3+}	–	–	–	–	0.86	0.86	–	–	0.19
Mn	–	–	–	–	0.01	0.01	0.01	–	0.05
Ti	–	–	–	–	0.34	0.34	0.32	0.01	0.22
Al^{iv}	1.02	1.02	1.02	1.02	1.16	1.16	1.21	1.05	1.19
Si	2.98	2.98	2.98	2.98	2.84	2.84	2.79	2.95	2.81
O	9.90	9.90	9.90	9.90	11.62	11.12	10.56	10.00	10.38
OH	0.16	0.16	0.16	0.16	0.21	0.71	1.13	0.70	1.38
F	1.94	1.94	1.94	1.94	0.17	0.17	0.08	1.30	0.22
Unit-cell data:									
a (Å)	5.307	5.318	5.326	5.335	5.320	5.331	5.357	5.308	5.389
b (Å)	9.195	9.207	9.230	9.233	9.210	9.231	9.245	9.190	9.324
c_i* (Å)	3.329	3.349	3.359	3.399	3.287	3.334	3.393	3.352	3.380
β (°)	100.1	100.1	100.1	100.0	100.1	100.2	95.0	100.1	100.6
α (°)	6.5	5.5	4.7	3.8	7.3	N.A.	5.3	7.5	1.6
V (Å^3)	87.98	87.98	87.98	87.98	84.96	84.96	87.92	85.24	86.38
V_i (Å^3)	162.46	163.98	165.13	167.43	161.07	164.07	168.04	163.51	169.74
Z_i (%)	45.84	46.34	46.72	47.45	47.25	48.21	47.68	47.87	49.11
P (bars)	1	1	1	1	1	1	1	1	1
T (°C)	25	202	400	600	25	25	25	25	25
Reference	G	G	G	G	H	H	I	J	J

independent substitutions listed above; this point extends to amphiboles as well (Dahl et al. 1995). Accordingly, the largest age discordance in the biotite-phlogopite series is predicted between F-phlogopite (Z=45.8%) and annite (Z=49.1%); see Table 4. These compositions could readily occur in adjacent metamorphic lithologies (e.g., in intercalated siliceous marbles and metapelites), and should be sought out as representing the best candidates for testing retention predictions within the trioctahedral mica sub-group.

Unequivocal geochronologic evidence for these predictions is scarce, because individual retentivity-composition effects themselves are either small, offsetting, or overwhelmed by tectonic/microstructural effects in many terranes. The latter complication is minimized in the remaining discussion by considering only those relative-age data from adjacent contrasting lithologies.

Permissive evidence for prediction (2) above (i.e., phlogopite older than annite) comes from data of Onstott et al. (1989), who observed older $^{40}Ar/^{39}Ar$ cooling ages for Mg-rich biotites than for adjacent Fe-richer analogues. They favored a Giletti-Norwood interpolation of Ar diffusivity as a function of Mg/Fe ratio in explaining their observation (cf., Giletti 1974a; Norwood 1974). Also, anecdotal evidence for predictions (2)–(4) (i.e., age variations within the ideal mica plane; Guidotti 1984) comes from the work of von Blanckenburg et al. (1989). They reported comparable K/Ar ages in biotites of quite *different* Mg/(Mg+Fe), but considered that some compensating chemical effect (unspecified) might allow the two biotites to share a common closure temperature. Indeed, their Fe-rich biotite (sample PJ-1) is also rich in Al^{vi}, whereas their Mg-rich biotite (sample PJ-9) is relatively Al^{vi}-poor; collectively, predictions (2)–(4) above lead to the suggestion that these two biotites had a common closure temperature. Perhaps significantly, further analysis now shows that the mean <K−O> values and overall unit-cell volumes of these two biotites are comparable too (ca. 2.90 ± 0.1 Å and 500 ± 1 Å^3, respectively, implying likewise comparable V_i and Z values). This is inferred by referencing the biotite compositions to contoured bond length and unit-cell volume variations in the ideal mica plane, as constrained by crystallographic data of Hewitt and Wones (1975) and Donnay et al. (1964). By itself, the fact of comparable <K−O> and unit-cell volumes in the two micas of von Blanckenburg et al. (1989) would suggest likewise comparable argon retention properties, according to the bond-length/strength arguments advanced in this paper.

Dioctahedral micas (muscovite, paragonite, and phengite)

Interrelationships among muscovite, paragonite, and phengite are dominated by the exchange vector components NaK_{-1} and $Al^{vi}Al^{iv}(Mg,Fe)_{-1}Si_{-1}$. Taken at face value, the tight clustering of most Z values (Z=44.5–46% at room conditions; Table 4) suggests that these dioctahedral micas have comparable Ar retention properties at given $P-T$ conditions. Relative-age data (albeit scarce) suitable for testing this hypothesis are considered below. First, for phengite-paragonite coexistences, Dallmeyer et al. (1990) observed the relative $^{40}Ar/^{39}Ar$ age sequence: phengite>paragonite (west-central Spitsbergen); yet Chopin and Maluski (1980) inferred just the opposite sequence (western Alps), which they rationalized in terms of basal spacings (c_i*). These conflicting sequences may reflect overlapping Z ranges for phengite and paragonite, which is permissive either of Z reversals between datasets or of relative dominance of diffusion-domain-size effects over minor Z effects. Alternatively, the relative-age comparison is open ended because only the data of Dallmeyer et al. (1990) unequivocally eliminate excess ^{40}Ar as a potential variable (i.e., in the form of concordant Rb/Sr and $^{40}Ar/^{39}Ar$ phengite ages). *Second*, among muscovite-paragonite coexistences described in the literature, none appear to have been dated radiometrically, so a direct test of the model is not yet possible. However, Hames (1994a) detected no evidence of an NaK_{-1} effect on $^{40}Ar/^{39}Ar$ closure ages of Acadian (Vermont) muscovites of widely variable Na content. Assuming that NaK_{-1} is the dominant variable in his dataset, extrapolation to paragonite suggests no significant difference in retentivity for natural compositions along the muscovite-paragonite join. This is consistent with the nearly identical Z values calculated in Table 4 for the equilibrium pair of sodic muscovite and potassic paragonite (Z=45.7 ± 0.3% and 45.4 ± 0.3%, respectively), which Burnham and Radoslovich (1964) extracted from a single hand specimen of a kyanite-schist from the Swiss Alps.

A much more common and important association of white micas is muscovite-phengite – typically a disequilibrium sub-assemblage in Alpine rocks, in which high-pressure phengite is overprinted by lower-pressure muscovite via discontinuous retrograde reactions (e.g., Ernst 1963). Relative isotopic ages of the two phases typically conform to this growth sequence (e.g., Wijbrans and McDougall 1986; Scaillet et al. 1992), such that Z comparisons are not particularly relevant as in the case of the presumably *equilibrium* sub-assemblages considered in prior discussion. Nevertheless, establishing relative (and absolute) Ar retention properties of these white micas remains crucial to interpretations of age data obtained from them (Arnaud and Kelley 1995), and the porosity model bears upon this issue directly. Specifically, the model predicts that: (1) Mg-rich phengites are more Ar retentive than their Fe-rich analogues, and (2) high lithostatic pressure (P) promotes Ar retention in micas generally. These predictions and supporting geochronologic evidence are considered further below.

Prediction (1) is consistent with the enhanced Ar retention indicated by preservation of older apparent $^{40}Ar/^{39}Ar$ ages in Mg-rich phengites (low Z inferred, this study) relative to Fe-rich analogues (higher Z) in adjacent metamorphic lithologies that experienced the same thermal history [Dora Maira Massif and environs, west-

ern Italian Alps: Scaillet et al. 1992 (see their Fig. 7); Monié and Chopin 1991 (cf., their Tables 1 and 2)]. In the current absence of c_i* data for phengites as a function of Fe/Mg ratio, however, positive correlation between Z and Fe/Mg ratio can only be inferred by extension from Fe−Mg solid solutions, wherein this trend is universally observed (e.g., garnet, pyroxene, hornblende, olivine, and biotite; Dahl 1994; see also Table 4). Scaillet et al. (1992) originally explained their retentivity-composition trend in terms of the reduced α-rotation and K−O bond strength brought about by a lithology-controlled $FeMg_{-1}$ substitution. Their explanation is fully compatible with the broader porosity model advanced here. Significantly, the model further predicts that the same relative phengite ages will arise *irrespective of the actual isotopic mass-transfer process involved*, our having argued above for biotite versus muscovite that K−O bond strength is the kinetic common denominator whereby all such processes tend to "pull" mica ages differentially in the same direction (other age-determining factors aside). It is important to add, however, that this crystal-chemical scenario cannot be advanced as a *unique* explanation of the relative phengite ages unless or until it is demonstrated that the adjacent phengite-bearing lithologies studied by Scaillet et al. (1992) were uniformly subjected to deformation, hydrothermal fluids, and excess argon (if any).

In any case, given compelling evidence that high-pressure (HP) metamorphism at Dora Maira culminated at ~38–50 Ma (Tilton et al. 1991; Arnaud and Kelley 1995), it is clear that only the Fe-rich (high-Z) phengites with their 35–40 Ma ages faithfully record this event ($P-T$ conditions of 10–20 kbar and 500–600° C; Scaillet et al. 1992). In contrast, the ≥90 Ma ages Scaillet et al. obtained from adjacent Mg-rich (lower-Z) phengites appear to indicate preservation of extraneous argon (either inherited or incorporated later). On the one hand, clustering of 90–115 Ma Mg-phengite ages in eclogites and blueschists at Dora Maira argues for inheritance (Monié and Chopin 1991); yet anomalously old ages obtained in the nearby metagranite prove the incorporation of excess ^{40}Ar (Arnaud and Kelley 1995). Locality-wide, however, these models are by no means mutually exclusive. What is important in terms of *this* study is that the retentivity difference documented by Scaillet et al. and its systematization in terms of Z nominally allows *either* geological interpretation.

Independent field evidence for a pressure effect on retention in dioctahedral micas [prediction (2) above] is restricted to: (1) the suggestion that high-P phengites close at higher T than low-P phengites (Monié and Chopin 1991), and (2) the general observation from the literature that extraneous argon seems to afflict high-P phengites more so than lower-P muscovites. Taken at face value, argon diffusion data for trioctahedral micas (Harrison et al. 1985; Giletti and Tullis 1977) also indicate a positive T_c-P dependence of ~4.3–7.6° C/kbar (i.e., ~1.2–2.3° C/km, assuming an average crustal density of 2.86 g/cm^3). A pressure dependence on T_c of this magnitude may reinforce fast cooling and non-zero partial pressure of Ar in explaining why HP phengites and biotites that coexisted in metagranite at ~575° C and 11 kbar (Arnaud and Kelley 1995) nevertheless were able partially to retain excess components incorporated at or near those conditions.

In developing a Z-based T_c-P prediction, it is important to note that previously we have treated only the *chemical* dependence of Z in coexisting minerals at given $P-T$ conditions. However, Z for a *given* mica depends also upon T and P, because its interlayer region contracts (and Z decreases) significantly upon either cooling or compression (Hazen 1985; see also Table 4). If Z in turn monitors diffusion kinetics, as argued in the previous section, then it follows on simple geometric grounds that isobaric cooling and isothermal compression *both* promote diffusional closure of argon in a mica structure by means of Z reduction; that is, there are closure *pressures* in addition to closure temperatures. We can calculate that interlayer Z for muscovite at room conditions (Table 4) is maintained along a $P-T$ trajectory of ca. 63° C/kbar (equivalent to ~18° C/km), according to recent expansion and compressibility data (Guggenheim et al. 1987; Comodi and Zanazzi 1995). Of course, any claim that this iso-Z contour also quantifies T_c-P behavior is exaggerated; instead, the 4.3–7.6° C/kbar (1.2–2.3° C/km) figure from diffusion data is far more tenable. The main point is that the two estimates agree in sign. Thus, porosity considerations independently predict that T_c and P are positively correlated, while also yielding insights into the geometric factors underlying this behavior at the atomic scale. A corollary distinction to be made is that closure in a mica is actually dictated by the crystal field (and monitoring Z) at elevated $P-T$, instead of that at room conditions, which has been our point of reference until now. Fortunately, there is good X-ray crystallographic evidence that ΔV_i (and thus ΔZ) values inferred between mica compositions at room conditions are approximately maintained at elevated P–T (Takeda and Morosin 1975; Hazen 1985; Guggenheim et al. 1987; Comodi and Zanazzi 1995), such that the retention differences modeled above in terms of 25° C Z values remain valid (see Table 4).

In summary, pressure effects on closure of HP micas may merit closer scrutiny, especially in light of 6–12° C/km pressure-temperature-depth trajectories characteristic of HP/LT Alpine terranes. The potentially shallow intersections of these paths and an iso-retentivity contour (whatever its actual slope and absolute position in $P-T$ space) could give rise to a wide array of effective closure temperatures for a given composition, depending upon the true magnitude of the pressure dependence.

Concluding remarks

1. It has been shown that interlayer spaciousness, vacancy concentration, and O−H bond orientation in micas determine the interlayer ionic porosity, Z – a measurable

parameter which in turn systematizes relative mica ages and other kinetics-related data. Thus, Z provides a first-order empirical link between Ar-loss/gain kinetics in micas and the governing geometric aspects of crystal chemistry. Although by no means without limitations, the ionic porosity approach (which builds upon earlier work of Dowty 1980 and Fortier and Giletti 1989) offers a simple, intuitively satisfying means of resolving the long debated age-composition question in mineral families. The need for an *empirical* modeling approach (whether porosity-based or otherwise) is dictated by the current lack of solutions to the Schrödinger wave equation (which theoretically would yield diffusion parameters for the micas) and by the paucity of experimental diffusion data for natural mica compositions of interest.

2. A significant conclusion of this paper is that relative-age patterns can arise irrespective of the dominant process(es) of isotopic loss in a terrane (volume diffusion, recrystallization, reaction, etc.). Moreover, these processes also appear to be mutually reinforcing in nature (e.g., Kelley 1988). It follows that any age discordance observed between muscovite (or phengite) and biotite cannot be ascribed *a priori* to any *one* process without appropriate field, petrographic, and petrologic constraint. This point raises some caution vis-à-vis strictly thermochronologic interpretation of age data for micas (and other minerals) in cooled igneous/metamorphic rocks, in which pure diffusion is implicitly assumed from a systematic progression of mineral ages [including muscovite (or phengite) $>$ biotite]. Even in the classic study of mineral-isotopic mass-transfer kinetics in a contact metamorphic zone, Hanson and Gast (1967) explicitly indicated that their spatial, inter-/intra-mineral age patterns for hornblende, muscovite, biotite, and feldspar could be explained either by volume diffusion or recrystallization (although the latter process is favored in similar rocks by Kelley and Turner 1991). Moreover, the dominant isotopic mass-transfer process may vary spatially and temporally within and among terranes, so even if volume diffusion of argon in micas is possible in one rock (e.g., as evidenced by grain scale, concentric age zonation; see Hodges et al. 1994, Hames 1994b), this result does not necessarily extend *beyond* that rock.

3. Where Ar loss has been dominated by diffusion, it seems unlikely that there is a single T_c for micas. Instead, it is more likely that a continuum of Ar retention behavior exists across mica compositional space (as also apparent in amphiboles; Dahl et al. 1995; Dahl in press; Kamber et al. 1995). Thus, the primary age-retention-composition relationship commonly observed between muscovite and biotite is considered to be augmented by secondary such trends among dioctahedral and trioctahedral varieties. Because age-composition relationships (particularly the secondary ones) may be variably obscured by tectonic, hydrothermal, microtextural, and excess-argon effects in nature, proper field testing of the predictions in this paper is best done in an "ideal end-member terrane" (Dahl et al. 1995; Dahl in press; Kamber et al. 1995). In such a terrane these complicating effects are minimized and cooling was sufficiently slow ($\leq$2–4° C/Ma) that closure-age differences preserved among adjacent micas will not have been compressed below analytical detection limits. Consequently, nature is most likely to have conducted a well-constrained diffusion experiment for us here, thus effectively isolating the compositional variables on retention postulated in this paper.

4. Finally, this paper should be viewed as a first effort to place the patterned observations of geochronology on firm crystal-chemical footing, and the empirical framework developed here may provide the basis for future calibration of a quantitative $T_c - Z$ scale for argon in micas (applicable were pure diffusion has dominated Ar loss). Pursuant to that goal, it is hoped that the current model will encourage and guide constrained field and laboratory experiments with which to test the predictions advanced herein, beginning with full crystal-chemical characterization of minerals subjected to dating and diffusion study. For now, however, the inverse $T_c - Z$ relationship for micas may be estimated at ca. 20–40° C ΔT_c for each 1% (absolute) ΔZ, judging from parallel study of amphiboles (Dahl et al. 1995; Dahl in press; Kamber et al. 1995).

Acknowledgements I thank many colleagues for useful discussions about mica crystal chemistry and its relationship to geochronology – including Drs. Robert Cliff, Darby Dyar, Ken Foland, Charles Guidotti, Daniel Holm, Simon Kelley, Daniel Lux, and Robert Wintsch. Special thanks are also due to Drs. Stéphane Scaillet and Igor Villa for their insightful, constructive reviews of the manuscript itself. Finally, I gratefully acknowledge research support for geochronology from the Homestake Mining Company and the Kent State University Foundation.

References

de Albuquerque CAR (1973) Geochemistry of biotites from granitic rocks, northern Portugal. Geochim Cosmochim Acta 37: 1779–1802

de Albuquerque CAR (1975) Partition of trace elements in co-existing biotite, muscovite, and potassium feldspar of granitic rocks, northern Portugal. Chem Geol 16: 89–108

Arnaud NO, Kelly SP (1995) Evidence for excess argon during high-pressure metamorphism in the Dora Maira Massif (western Alps, Italy), using an ultra-violet laser ablation microprobe ^{40}Ar–^{39}Ar technique. Contrib Mineral Petrol (in press)

Bailey SW (1984) Crystal chemistry of the true micas. In: Bailey SW (ed) Micas. (Reviews in mineralogy, vol 10) Mineral Soc Am, Washington, DC, pp 13–60

Baños JO, Amouric M, de Fouquet C, Baronnet A (1983) Interlayering and interlayer slip in biotite as seen by HRTEM. Am Mineral 68: 754–758

Bassett WA (1960) Role of hydroxyl orientation in mica alteration. Geol Soc Am Bull 71: 449–456

Berry RF, McDougall I (1986) Interpretation of $^{40}Ar/^{39}Ar$ and K/Ar dating evidence from the Aileu Formation, East Timor. Chem Geol Isot Geosci 59: 43–58

von Blanckenburg F, Villa IM, Baur H, Morteani G, Steiger RH (1989) Time calibration of a *PT*-path from the western Tauern Window, eastern Alps: the problem of closure temperatures. Contrib Mineral Petrol 101: 1–11

Bohlen SR, Peacor DR, Essene EJ (1980) Crystal chemistry of a metamorphic biotite and its signnificance in water barometry. Am Mineral 65: 55–62

Boles JR, Johnson KS (1983) Influences of mica surfaces on pore-water pH. Chem Geol 43: 303–317

Brewer MS (1969) Excess radiogenic argon in metamorphic micas from the eastern Alps, Austria. Earth Planet Sci Lett 6: 321–331

Brodie KH, Rutter EH (1985) On the relationship between deformation and metamorphism, with special reference to the behavior of basic rocks. In: Thompson AB, Rubie DC (eds) Metamorphic reactions: kinetics, textures, and deformation. (Advances in physical geochemistry, vol 4). Springer, Berlin Heidelberg New York, pp 138–179

Burnham CW, Radoslovich EW (1964) Crystal structures of coexisting muscovite and paragonite. Carnegie Inst Washington Year 63: 232–236

Chopin C, Maluski H (1980) $^{40}Ar/^{39}Ar$ dating of high-pressure metamorphic micas from the Gran Paradiso area (western Alps): evidence against the blocking temperature concept. Contrib Mineral Petrol 74: 109–122

Circone S, Navrotsky A, Kirkpatrick RJ, Graham CM (1991) Substitution of $^{[6,4]}Al$ in phlogopite: mica characterization, unit-cell variation, ^{27}Al and ^{29}Si MAS-NMR spectroscopy, and Al−Si distribution in the tetrahedral sheet. Am Mineral 76: 1485–1501

Clauer N (1981) Strontium and argon isotopes in natural weathered biotites, muscovites and feldspars. Chem Geol 31: 325–334

Cliff RA, Droop GTR, Rex DC (1985) Alpine metamorphism in the south-east Tauern Window, Austria. 2. Rates of heating, cooling and uplift. J Metamorphic Geol 3: 403–415

Comodi P, Zanazzi PF (1995) High-pressure structural study of muscovite. Phys Chem Mineral 22: 170–177

Cruciani G, Zanazzi PF (1994) Cation partitioning and substitution mechanisms in 1*M* phlogopite: a crystal-chemical study. Am Mineral 79: 289–301

Dahl PS (1994) "Ionic porosity" as a predictor of diffusion parameters in thermochronometric minerals: evidence and tectonic impliations (abstract). Mineral Mag 58A:205–206

Dahl PS (1995) An "ionic porosity" approach to modeling compositional effects on Ar and O retentivity in thermochronometric minerals: applications to clino-amphiboles. Geochim Cosmochim Acta (in press)

Dahl PS, Dorais M (1995) The influence of $F(OH)_{-1}$ substitution on the relative mechanical strength of rock-forming micas. J Geophys Res (in press)

Dahl PS, Wehn DC, Feldmann SG (1993) The systematics of trace-element partitioning between coexisting muscovite and biotite in metamorphic rocks from the Black Hills, South Dakota, U.S.A.. Geochim Cosmochim Acta 57: 2487–2505

Dahl PS, Kamber BS, Villa IM (1995) Field test of a retentivity-composition model for argon in hornblende: implications for thermochronology (abstract). Trans Am Geophys Union EOS 76:S 285

Dallmeyer RD, Gee DG (1986) $^{40}Ar/^{39}Ar$ mineral dates from retrogressed eclogites within the Baltoscandian miogeocline: implications for a polyphase Caledonian orogenic evolution. Geol Soc Am Bull 97: 26–34

Dallmeyer RD, Peucat JJ, Hirajina T, Ohta Y (1990) Tectonothermal chronology within a blueschist-eclogite complex, west-central Spitsbergen, Svalbard: evidence from $^{40}Ar/^{39}Ar$ and Rb−Sr mineral ages. Lithos 24: 291–304

Deer WA, Howie RA, Zussman J (1963) Sheet silicates. (Rock forming minerals, vol 3) John Wiley and Sons, New York

Dodson MH (1973) Closure temperatures in cooling geochronological and petrological systems. Contrib Mineral Petrol 40: 259–274

Dodson MH (1975) Diffusion effects of a thermal pulse (abstract). Trans Am Geophys Union EOS 56: 472

Dodson MH (1986) Closure profiles in cooling systems. Mater Sci Forum 7: 145–154

Donnay G, Donnay JDH, Takeda H (1964) Trioctahedral one-layer micas. II. Prediction of the structure from composition and cell dimensions. Acta Crystallogr 17: 1374–1381

Dowty E (1980) Crystal-chemical factors affecting the mobility of ions in minerals. Am Mineral 65: 174–182

Dutrow BL, Holdaway MJ, Hinton RW (1986) Lithium in staurolite and its petrologic significance. Contrib Mineral Petrol 94: 496–506

Dyar MD, Colucci MT, Guidotti CV (1991) Forgotten major elements: hydrogen and oxygen variation in biotite from metapelites. Geology 19: 1029–1032

Dymek RF (1983) Titanium, aluminum, and interlayer-cation substitutions in biotite from high-grade gneisses, west Greenland. Am Mineral 68: 880–899

Ernst WG (1963) Significance of phengitic micas from low-grade schists. Am Mineral 63: 621–640

Evans BW (1969) Chlorine and fluorine in micas of pelitic schists from the sillimanite-orthoclase isograd, Maine. Am Mineral 54: 1209–1211

Farmer VC, Russell JD, McHardy WJ, Newman ACD, Ahlrichs JL, Rimsaite JYH (1971) Evidence for loss of protons and octahedral iron from oxidized biotites and vermiculites. Mineral Mag 38: 121–127

Faure G (1986) Principles of isotope geochemistry. John Wiley and Sons, New York

Fletcher CJN, Greenwood HJ (1979) Metamorphism and structure of the Penfold Creek area, near Quesnal Lake, British Columbia. J Petrol 20: 743–794

Foland KA (1983) $^{40}Ar/^{39}Ar$ incremental heating plateaus for biotites with excess argon. Chem Geol Isot Geosci 1: 3–21

Fortier SM, Giletti BJ (1989) An empirical model for predicting diffusion coefficients in silicate minerals. Science 245: 1481–1484

Fortier SM, Giletti BJ (1991) Volume self-diffusion of oxygen in biotite, muscovite, and phlogopite micas. Geochim Cosmochim Acta 55: 1319–1330

Gaber LJ, Foland KA, Carbato CE (1988) On the significance of argon release from biotite and amphibole during $^{40}Ar/^{39}Ar$ vacuum heating. Geochim Cosmochim Acta 52: 2457–2465

Giese RF (1979) Hydroxyl orientation in 2: 1 phyllosilicates. Clays Clay Miner 27: 213–223

Giese RF (1984) Electrostatic energy models of micas. In: Bailey SW (ed) Micas. (Reviews in mineralogy, vol 10) Mineral Soc Am, Washington, DC, pp 105–144

Giletti BJ (1974a) Studies in diffusion. I. Argon in phlogopite mica. In: Hofmann AW, Giletti BJ, Yoder HS, Yund RA (eds) Geochemical transport and kinetics. Carnegie Inst Washington Publ 634, pp 107–115

Giletti BJ (1974b) Diffusion related to geochronology. In: Hofmann AW, Giletti BJ, Yoder HS, Yund RA (eds) Geochemical transport and kinetics. Carniegie Inst Washington Publ 634, pp 61–76

Giletti BJ, Tullis J (1977) Studies in diffusion. IV. Pressure dependence of Ar diffusion in phlogopite mica. Earth Planet Sci Lett 35: 180–183

Goodwin LB, Renne PR (1991) Effects of progressive mylonitization on Ar retention in biotites from the Santa Rosa mylonite zone, California, and thermochronologic implications. Contrib Mineral Petrol 108: 283–297

Graham CM, Elphick SC (1991) Some experimental constraints on the role of hydrogen and oxygen diffusion and Al−Si interdiffusion in silicates. In: Ganguly J (ed) Diffusion, atomic ordering, and mass transport. Springer, Berlin Heidelberg New York, pp 248–285

Grove M, Harrison TM (1993) Compositional controls governing argon loss in biotite (abstract). Trans Am Geophys Union EOS 74: 339

Grove M, Harrison TM (1994) Argon loss from F−OH phlogopite (abstract). US Geol Surv Circ 1107: 119

Guggenheim S (1984) The brittle micas. In: Bailey SW (ed) Micas. (Reviews in mineralogy, vol 10) Mineral Soc Am, Washington, DC, pp 61–104

Guggenheim S, Chang Y-H, Koster von Groos AK (1987) Muscovite dehydroxylation: high-temperature studies. Am Mineral 72: 537–550

Guidotti CV (1984) Micas in metamorphic rocks. In: Bailey SW (ed) Micas. (Reviews in mineralogy, vol 10). Mineral Soc Am,Washington, DC, pp 357–467

Guidotti CV, Dyar MD (1991) Ferric iron in metamorphic biotite and its petrologic and crystallochemical implications. Am Mineral 76: 161–175

Güven N (1971) The crystal structure of $2M_1$ phengite and $2M_1$ muscovite. Z Kristallogr 125: 1–6

Hames WE (1994 a) An empirical study of factors controlling ^{40}Ar retention in muscovite from the Gassetts schist, Vermont Appalachians (abstract). US Geol Surv Circular 1107: 123

Hames WE (1994 b) The dynamic range of argon retention in single crystals, examples for muscovite across the Acadian metamorphic field gradient in western New England (abstract). US Geol Surv Circular 1107: 123

Hames WE, Bowring SA (1994) An empirical evaluation of the argon diffusion geometry of muscovite. Earth Planet Sci Lett 124: 161–167

Hanson GL, Gast PW (1967) Kinetic studies in contact metamorphic zones. Geochim Cosmochim Acta 31: 1119–1153

Harlow GE (1991) Barium enriched true micas from metasomatized inclusions in serpentinite, Motagua Valley, Guatemala (abstract). Geol Soc Am Abstr Program 23(5):A219

Harlow GE (1995) Crystal chemistry of barian micas. Eur J Mineral (in press)

Harrison TM, Duncan I, McDougall I (1985) Diffusion of ^{40}Ar in biotite: temperature, pressure and compositional effects. Geochim Cosmochim Acta 49: 2461–2468

Hazen RM (1985) Comparative crystal chemistry and the polyhedral approach. In: Kieffer SW, Navrotsky A (eds) Microscopic to macroscopic: atomic environments to mineral thermodynamics. (Reviews in mineralogy, vol 14) Mineral Soc Am, Washington, DC, pp 317–346

Hazen RW, Burnham CW (1973) The crystal structure of one-layer phlogopite and annite. Am Mineral 58: 889–900

Hervig RL, Peacock SM (1989) Water and trace elements in coexisting muscovite and biotite from metamorphic rocks (abstract). Trans American Geophys Union EOS 70: 490

Hewitt CT, Wones DR (1975) Physical properties of some synthetic Fe−Mg−Al trioctahedral biotites. Am Mineral 60: 854–862

Hodges KV, Spear FS (1982) Geothermometry, geobarometry and the Al_2SiO_5 triple point at Mt. Moosilauke, New Hampshire. Am Mineral 67: 1118–1134

Hodges KV, Hames WE, Bowring SA (1994) $^{40}Ar/^{39}Ar$ age gradients in micas from a high-temperature-low-pressure metamorphic terrain: evidence for very slow cooling and implications for the interpretation of age spectra. Geoloy 22: 55–58

Hoisch TD (1989) A muscovite-biotite geothermometer. Am Mineral 74: 565–572

Joswig W, Takéuchi Y, Fuess H (1983) Neutron-diffraction study on the orientation of hydroxyl groups in margarite. Z Kristallogr 165: 295–303

Kamber BS, Blenkinsop TG, Villa IM, Dahl PS (1995) Proterozoic transpressive deformation in the northern Marginal Zone, Limpopo belt, Zimbabwe. J Geol 103: 493–508

Kelley SP (1988) The relationship between K−Ar mineral ages, mica grainsizes and movement on the Moine thrust zone, NW Highlands, Scotland. J Geol Soc London 145: 1–10

Kelley SP, Bluck BJ (1992) Laser ^{40}Ar–^{39}Ar ages for individual detrital muscovites in the Southern Uplands of Scotland, U.K. Chem Geol Isot Geosci 101: 143–156

Kelley SP, Turner G (1991) Laser probe ^{40}Ar-^{39}Ar measurements of loss profiles within individual hornblende grains from the Giants Range granite, northern Minnesota, USA. Earth Planet Sci Lett 107: 634–648

Kronenberg AK, Kirby SH, Pinkston J (1990) Basal slip and mechanical anisotropy of biotite. J Geophys Res 95-B:19 257–19 278

Laperche V (1991) Etude de l'état et de la délocalisation des cations compensateurs dans les phyllosilicates. Thèse, Univ Paris VII, France

Larsen SJ, Pardoe GWF, Gebbie HA (1972) The use of far infrared interferometric spectroscopy for mineral identification. Am Mineral 57: 998–1002

Lasaga AC (1981) The atomistic basis of kinetics: defects in minerals. In: Lasaga AC, Kirkpatrick RJ (eds) Kinetics of geochemical processes. (Reviews in mineralogy, vol 8) Mineral Soc Am, Washington, DC, pp 261–319

Lin C-Y, Bailey SW (1984) The crystal structure of paragonite-$2M_1$. Am Mineral 69: 122–127

Lo C-H (1988) Chloritization of biotite in the granitic rocks of eastern Taiwan and its implications for isotope geochronology. Acta Taiwanica 26: 291–315

Lo C-H, Onstott TC (1989) ^{39}Ar recoil artifacts in chloritized biotite. Geochim Cosmochim Acta 53: 2697–2711

Loucks RR (1991) The bound interlayer H_2O content of potassic white micas: muscovite-hydromuscovite-hydrophyllite solutions. Am Mineral 76: 1563–1579

Manning JR (1974) Diffusion kinetics and mechanisms in simple crystals. In: Hofmann AW, Giletti BJ, Yoder HS, Yund RA (eds) Geochemical transport and kinetics. Carnegie Inst Washington Publ 634, p 3–13

Mansker WL, Ewing RC, Keil K (1979) Barian-tetanian biotites in nephelinites from Oahu, Hawaii. Am Mineral 64: 156–159

Mares VM, Kronenberg AK (1993) Experimental deformation of muscovite. J Struct Geol 15: 1061–1075

McDougall I, Harrison TM (1988) Geochronology and thermochronology by the $^{40}Ar/^{39}Ar$ method. Oxford University Press, Oxford

Meike A (1989) In situ deformation of micas: a high-voltage electron-microscope study. Am Mineral 62: 304–308

Mitchell JG, Taka AS (1984) Potassium and argon loss patterns in weathered micas: implications for detrital mineral studies, with particular reference to the Triassic palaeogeography of the British Isles. Sediment Geol 39: 27–52

Mitchell JG, Penven M-J, Ineson PR, Miller JA (1988) Radiogenic argon and major-element loss from biotite during natural weathering: a geochemical approach to the interpretation of potassium-argon ages of detrital biotite. Chem Geol Isot Geosci 72: 111–126

Moloshag VP, Teremetskaya AG (1975) Cesium-bearing biotite in host rocks of one rare-metal pegmatite field. Dokl Acad Sci USSR Earth Sci 221: 137–139

Monié P, Chopin C (1991) $^{40}Ar/^{39}Ar$ dating in coesite-bearing and associated units of the Dora Maira massif, western Alps. Eur J Mineral 3: 239–262

Munoz JL, Ludington SD (1977) Fluorine-hydroxyl exchange in biotite. Am Mineral 62: 304–308

Nemec D (1980) Fluorine phengites from tin-bearing orthogneisses of the Bohemian-Moravian Heights, Czechoslovakia. Neues Jahrb Mineral Abh 139: 155–169

Norrish K (1973) Factors in the weathering of mica to vermiculite. In: Serratosa JM (ed) 1972 Proc Int Clay Conf Div Cienc, Madrid, pp 417–432

Norwood CB (1974) Radiogenic argon diffusion in the biotite micas. MS thesis, Brown Univ, USA

Ohta T, Takeda H, Takéuchi Y (1982) Mica polytypism: similarities in the crystal structures of coexisting $1M$ and $2M_1$ oxybiotite. Am Mineral 67: 298–310

Onstott TC, Peacock MW (1987) Argon retentivity of hornblendes: a field experiment in a slowly cooled metamorphic terrane. Geochim Cosmochim Acta 51: 2891–2903

Onstott TC, Hall CM, York D (1989) $^{40}Ar/^{39}Ar$ thermochronometry of the Imataca complex, Venezuela. Precambrian Res 42: 255–291

Onstott TC, Phillips D, Pringle-Goodell L (1991) Laser microprobe measurement of chlorine and argon zonation in biotite. Chem Geol 90: 145–168

Papike JJ, Shearer CK, Simon SB, Laul JC (1984) Crystal-chemical aspects of Li, Rb, and Cs partitioning between coexisting muscovite and biotite (abstract). 27th Int Geol Congr Moscow 5: 135

Phillips D, Onstott TC (1988) Argon isotopic zoning in mantle phlogopite. Geology 16: 542–546
Putnis A (1992) Introduction to mineral sciences. Cambridge University Press, Cambridge
Rambaldi ER (1973) Variation in the composition of muscovite and biotite in some metamorphic rocks near Bancroft, Ontario. Can J Earth Sci 10: 869–880
Reddy SM, Kelley WP, Wheeler J (1995) A $^{40}Ar/^{39}Ar$ laser probe study of micas from the Sesia Zone, western Alps: implications for metamorphic and deformation histories. Earth Planet Sci Lett (in press)
Robbins GA (1972) Radiogenic argon diffusion in muscovite under 3 hydrothermal conditions. MS thesis, Brown Univ, USA
Rubie DC, Thompson AB (1985) Kinetics of metamorphic reactions at elevated temperatures and pressures: an appraisal of available experimental data. In: Thompson AB, Rubie DC (eds) Metamorphic reactions: kinetics, textures, and deformation. (Advances in physical geochemistry, vol 4). Springer, Berlin Heidelberg New York, pp 27–79
Scaillet S, Féraud G, Ballèvre M, Amouric M (1992) Mg/Fe and $[(Mg,Fe)Si-Al_2]$ compositional control on argon behavior in high-pressure white micas: $^{40}Ar/^{39}Ar$ continuous laser-probe study from the Dora Maira nappe of the internal western Alps, Italy. Geochim Cosmochim Acta 56: 2851–2872
Serratosa JM, Bradley WF (1958) Determination of the orientation of OH bond axes in layer silicates by infrared absorption. J Phys Chem 62: 1164–1167
Shannon RD (1976) Revised effective ionic radii and systematic studies of interatomic distances in halides and chalcogenides. Acta Crystallogr A32: 751–767
Shearer CK, Papike JJ, Simon SB, Laul JC (1986) Pegmatite-wallrock interaction, Black Hills, South Dakota: interaction between pegmatite-derived fluids and quartz-mica schist wallrock. Am Mineral 71: 518–539
Takeda H, Morosin B (1975) Comparison of observed and predicted structural parameters of mica at high temperature. Acta Crystallogr B31: 2444–2452
Tilton GR, Schreyer W, Schertl H-P (1991) Pb–Sr–Nd isotopic behavior of deeply subducted crustal rocks from the Dora Maira Massif, western Alps, Italy. II. What is the age of the ultrahigh-pressure metamorphism? Contrib Mineral Petrol 108: 22–33
Tracy RJ (1978) High-grade metamorphic reactions and partial melting in pelitic schist, west central Massachusetts. Am J Sci 278: 150–178
Tracy RJ (1991) Ba-rich micas from the Franklin Marble, Lime Crest and Sterling Hill, New Jersey. Am Mineral 76: 1683–1693
Vaughan MT, Guggenheim S (1986) Elasticity of muscovite and its relationship to crystal structure. J Geophys Res 91(B5):4657–4664
Veblen D (1980) Anthophyllite asbestos: microstructures, intergrown sheet silicates, and mechanisms of fiber formation. Am Mineral 65: 1075–1086
Vernon RH (1977) Microfabric of mica aggregates in partly recrystallized biotite. Contrib Mineral Petrol 61: 175–185
Villa IM (1991) Excess Ar geochemistry in potassic volcanites. Schweiz Mineral Petrogr Mitt 71: 211–225
Villa IM, Puxeddu M (1994) Geochronology of the Larederello geothermal field: new data and the "closure temperature" issue. Contrib Mineral Petrol 115: 415–426
Volfinger M (1976) Effet de la température sur les distributions de Na, Rb, et Cs entre le sanidine, la muscovite, la phlogopite, et une solution hydrothermale sous une pression de 1 kbar. Geochim Cosmochim Acta 40: 267–282
Voltaggio M (1985) Estimation of diffusion constants by observations of isokinetic effects: a test for radiogenic argon and strontium. Geochim Cosmochim Acta 49: 2117–2122
Walther JV, Wood BJ (1986) Mineral-fluid reaction rates. In: Walther JV, Wood BJ (eds) Fluid-rock interactions during metamorphism. (Advances in physical geochemistry, vol 5). Springer, Berlin Heidelberg New York, pp 194–211
Wendlandt RF (1977) Barium-phlogopite from Haystack Butte, Highwood Mountains, Montana. Carnegie Inst Washington Yearb 76: 534–539
Wijbrans JR, McDougall I (1986) $^{40}Ar/^{39}Ar$ dating of white micas from an Alpine high-pressure metamorphic belt on Naxos (Greece): the resetting of the argon isotopic system. Contrib Mineral Petrol 93: 187–194
Wilson CJL, Bell IA (1979) Deformation of biotite and muscovite: optical microstructure. Tectonophysics 58: 179–200
Wones DR (1963) Phase equilibria of "ferriannite" $KFe_3+2Fe+3Si_3O_{10}(OH)_2$. Am J Sci 261: 581–596
Yoder HS, Eugster HP (1954) Phlogopite synthesis and stability range. Geochim Cosmochim Acta 6: 157–185
Zimmermann JL (1970) Contribution a l'étude de la déshydration et de la liberation de l'argon des micas. Geochim Cosmochim Acta 34: 1327–1350